Electronic structure of $YbGa_{1.15}Si_{0.85}$ and $YbGa_xGe_{2-x}$ probed by resonant x-ray emission and photoelectron spectroscopies

Hitoshi Yamaoka,[1] Ignace Jarrige,[2] Naohito Tsujii,[3] Motoharu Imai,[4] Jung-Fu Lin,[5] Masaharu Matsunami,[6] Ritsuko Eguchi,[7] Masashi Arita,[8] Kenya Shimada,[8] Hirofumi Namatame,[8] Masaki Taniguchi,[8] Munetaka Taguchi,[1] Yasunori Senba,[9] Haruhiko Ohashi,[9] Nozomu Hiraoka,[10] Hirofumi Ishii,[10] and Ku-Ding Tsuei[10]

[1]*Harima Institute, RIKEN (The Institute of Physical and Chemical Research), Sayo, Hyogo 679-5148, Japan*
[2]*Japan Atomic Energy Agency, SPring-8 1-1-1 Kouto, Sayo, Hyogo 679-5148, Japan*
[3]*Quantum Beam Center, National Institute for Materials Science, 1-2-1 Sengen, Tsukuba 305-0047, Japan*
[4]*Advanced Electronic Materials Center, National Institute for Materials Science, 1-2-1 Sengen, Tsukuba 305-0047, Japan*
[5]*Department of Geological Sciences, The University of Texas at Austin, Austin, Texas 78712, USA*
[6]*Institute for Molecular Science, Myodaiji, Okazaki 444-8787, Japan*
[7]*Faculty of Science, Okayama University, Okayama 700-8530, Japan*
[8]*Hiroshima Synchrotron Radiation Center, Hiroshima University, Higashi-Hiroshima, Hiroshima 739-0046, Japan*
[9]*Japan Synchrotron Research Institute, Sayo, Hyogo 679-5148, Japan*
[10]*National Synchrotron Radiation Research Center, Hsinchu 30076, Taiwan*

(Received 9 November 2010; revised manuscript received 28 January 2011; published 31 March 2011)

We performed an x-ray spectroscopic study combining resonant x-ray emission spectroscopy (RXES) and photoelectron spectroscopy on the superconducting ternary silicide $YbGa_{1.15}Si_{0.85}$ and nonsuperconducting ternary germanide $YbGa_xGe_{2-x}$ ($x = 1.0$ and 1.1). The Yb valence for all three compounds is found to be about 2.3. In $YbGa_{1.15}Si_{0.85}$ no temperature dependence of the Yb valence is observed in the RXES spectra in the temperature range of 7–300 K, while the valence shows a drastic increase under pressure from the Yb^{2+} state partially including itinerant electrons to the localized Yb^{3+} state. Differences are observed in the valence-band spectra of the photoelectron spectroscopy between $YbGa_{1.15}Si_{0.85}$ and $YbGa_xGe_{2-x}$, which may be attributed to the difference of crystal structure. We conclude that both the crystal structure of the planar GaSi layer in $YbGa_{1.15}Si_{0.85}$ and the resultant electronic structure may have a crucial role in the occurrence of superconductivity.

DOI: 10.1103/PhysRevB.83.104525 PACS number(s): 74.70.Dd, 75.30.Mb, 79.60.−i, 78.70.En

I. INTRODUCTION

Layered structure is considered to play an important role in the superconductivity of superconductors with AlB_2-type structure. In MgB_2 (superconducting transition temperature $T_C = 39$ K) the B atoms form a honeycomb layer and the Mg atoms are intercalated between the B layers.[1] Superconductivity with other layered materials has been reported in the graphite intercalation compounds of CaC_6 ($T_C = 11.5$ K) and YbC_6 ($T_C = 6.5$ K) (Refs. 2 and 3). In these materials C atoms form the honeycomb layer and Ca or Yb atoms are located between the layers. Ternary silicides with the AlB_2-type structure also showed superconductivity.[4–8] The superconductivity was also related to the lattice parameter within the layer rather than the interlayer spacing as shown in MAlSi (M = Ca, Sr, Ba) (Ref. 9). Inelastic x-ray scattering for CaAlSi suggested soft-phonon-driven superconductivity (i.e., a conventional BCS superconductor in the weak coupling regime.[10])

Recently the ternary rare-earth silicide, $YbGa_{1.1}Si_{0.9}$, has been found to be a type-II superconductor with $T_C = 2.4$ K and hexagonal AlB_2-type crystal structure.[11] A magnetic susceptibility measurement suggested that Yb of $YbGa_{1.1}Si_{0.9}$ was divalent with a small fraction of Yb^{3+}. Tsujii *et al.*[12] observed that T_C decreases with increasing x between $x = 1.1$ and 1.4. Magnetic susceptibility showed almost nonmagnetic character, indicating nearly divalent Yb valence, while the valence was measured to be 2.3 by x-ray absorption spectroscopy (XAS). It is, however, not clear yet to which extent the mixed-valence state and the superconductivity are linked.

On the other hand, the isoelectronic compound YbGaGe does not show superconductivity. YbGaGe has hexagonal structure with YPtAs type. A similar structural relation takes place for EuGaSi (AlB_2 type) and EuGaGe (YPtAs type), although $EuGa_xSi_{2-x}$ ($0.276 \leqslant x \leqslant 1.67$) does not show superconductivity down to 2 K (Ref. 13). It is noted that in YbGaSi the GaSi layer is flat, but in YbGaGe the GaGe sheets are no longer planar. Several authors reported the magnetic and electronic properties of YbGaGe (Refs. 14–20). By XAS the Yb valence of YbGaGe was found to be nearly divalent and constant with temperature.[21] Such temperature dependence of the electronic structure for YbGaSi has not been explored yet, nor the pressure dependence. It is not clear yet whether the absence of superconductivity in YbGaGe is primarily due to differences in the electronic or crystal structure compared with YbGaSi. To address this issue, we performed a detailed investigation of the electronic structure of superconducting $YbGa_{1.15}Si_{0.85}$ and nonsuperconducting $YbGa_xGe_{2-x}$ ($x =$ 1.0 and 1.1), using a combination of resonant x-ray emission spectroscopy (RXES), x-ray absorption spectroscopy in the partial fluorescence mode (PFY-XAS),[22–28] and soft x-ray and vacuum ultraviolet (UV) photoelectron spectroscopy (PES).[29,30] No temperature dependence of the valence was found for $YbGa_{1.15}Si_{0.85}$, while the valence was found to increase dramatically with pressure. Our results indicate that the valence does not show a significant difference between

$YbGa_xSi_{2-x}$ and YbGaGe, but the valence-band spectra are different, which may be attributed to the difference in the crystal structure.

II. EXPERIMENTS

We prepared $YbGa_{1.15}Si_{0.85}$, $YbGa_{1.1}Ge_{0.9}$, and YbGaGe synthesized by arc melting and annealing.[12] Chemical compositions are determined by using electron probe microanalysis. The atomic ratio Yb : (Ga + Si) is almost 1 : 2 in these compounds. Therefore hereafter we will neglect the deficiency in Yb site and write the chemical composition just as $YbGa_{1.15}Si_{0.85}$. The $YbGa_xSi_{2-x}$ ($1.12 \leqslant x \leqslant 1.49$) samples have been disclosed as type-II superconductors,[11,12] for an example, with $T_C = 2.4$ K at $x = 1.1$, while $YbGa_{1.1}Ge_{0.9}$ and YbGaGe are nonsuperconductors.[12] In $YbGa_xSi_{2-x}$ x-ray diffraction study showed that the AlB_2 structure phase was stabilized between $1.12 \leqslant x \leqslant 1.49$. Hereafter sometimes we simply describe this compound as YbGaSi for clarity. At $x = 1.0$ the diffraction pattern showed AlB_2-type (space group $P6/mmm$) phase mainly and $YbSi_{2-\delta}$ phase partially.[12] Lattice parameters were measured to be $a = 4.1275$ Å and $c = 4.2357$ Å for $YbGa_{1.1}Si_{0.9}$ (Refs. 11 and 12). In $YbGa_xSi_{2-x}$ at the range from $x = 1.15$ to $x = 1.4$ T_C decreases monotonically with increasing x while the volume increases.[12]

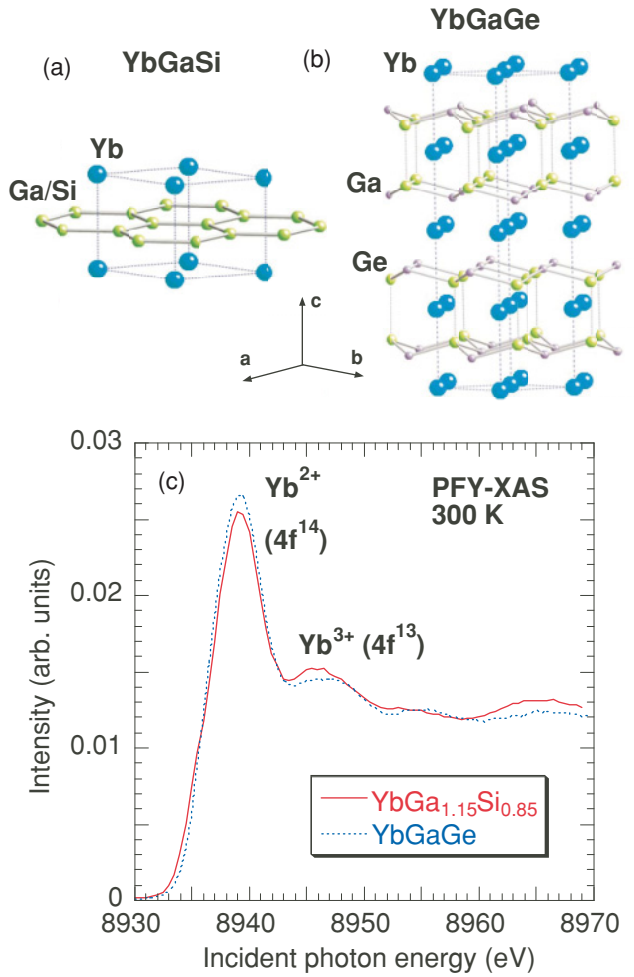

FIG. 1. (Color online) Crystal structures of (a) YbGaSi and (b) YbGaGe. (c) PFY-XAS spectra of $YbGa_{1.15}Si_{0.85}$ (solid line), and YbGaGe (dashed line) at 300 K.

Figures 1(a) and 1(b) show crystal structures of $YbGa_{1.15}Si_{0.85}$ and YbGaGe. In $YbGa_xSi_{2-x}$ randomly arranged Ga and Si atoms form a honeycomb layer and Yb atoms are intercalated into the space between the flat Ga-Si layer. The YbGaGe compound has the hexagonal YPtAs-type (space group $P6_3/mmc$) structure. This also has a layered structure consisting of a puckered Ga-Ge plane sandwiched between Yb planes, which is derived from the AlB_2-type structure by a systematic puckering of the Ga-Ge layers to form the four-fold periodicity in the stacking sequence of the layer along the c axis.

PFY-XAS and RXES measurements were performed at the Taiwan beamline BL12XU, SPring-8.[22,27,28] The undulator beam was monochromatized by a pair of cryogenically cooled Si(111) crystals and focused to a size of 20(horizontal) × 50(vertical) μm^2 at the sample position using toroidal and Kirkpatrick-Baez mirrors. Incident photon flux was estimated to be about 8×10^{12} photons/s at 8.9 keV from the measurement by using a pin-diode (type S3590-09). A Johann-type spectrometer equipped with a spherically bent Si(620) crystal (radius of ~1 m) was used to analyze the Yb $L\alpha_1$ ($3d_{5/2} \rightarrow 2p_{3/2}$) and Raman emissions with a solid state detector (XFlash 1001 type 1201). The overall energy resolution was estimated to be about 1 eV around the emitted photon energy of 7400 eV from the elastic scattering. The intensities of all spectra are normalized by the incident beam intensity monitored just before the target. A closed-circuit He cryostat was used for the low-temperature measurements down to 7 K. The high-pressure conditions were realized using a diamond anvil cell with a Be gasket and the pressure-transmitting medium was silicone oil. The pressure was measured based on the Raman shift of the ruby fluorescence.

Soft x-ray and UV PES were performed at the undulator beamlines, BL17SU of SPring-8 in Nishi-Harima[29] and BL9A of HiSOR in Hiroshima university[31] in Japan, with hemispherical electron analyzers SCIENTA SES 2002. In the soft x-ray PES the resolution, ΔE, was estimated to be about 200 meV at the incident photon energy of $E_{in} = 1100$ eV, estimated from Au valence spectra. The measurements were performed on clean surfaces by fracturing the samples at 45–50 K under the vacuum pressure below 3–5 × 10^{-8} Pa. In the UV PES ΔE was less than about 10 meV at $E_{in} = 9$ and 35 eV under the vacuum pressure below 2 × 10^{-9} Pa. Au $4f$ lines and Fermi edge were used to correct the measured photoelectron energy. In the UV PES the samples were also fractured before the measurements.

III. RESULTS AND DISCUSSION

A. PFY-XAS and RXES at ambient pressure

We start with the PFY-XAS and RXES spectra measured at 300 K and ambient pressure. Figure 1(c) shows the PFY-XAS spectra measured for $YbGa_{1.15}Si_{0.85}$ and YbGaGe, with the crystal structures of YbGaSi [Fig. 1(a)] and YbGaGe [Fig. 1(b)]. The PFY-XAS spectra are normalized in intensity by their area. The spectra show that these compounds are in the mixed valence state. The PFY-XAS spectra consist of a main Yb^{2+} ($4f^{14}$) peak at $E_{in} = 8939$ eV and a smaller peak corresponding to Yb^{3+} ($4f^{13}$) around $E_{in} = 8945$ eV. The difference between these spectra is small.

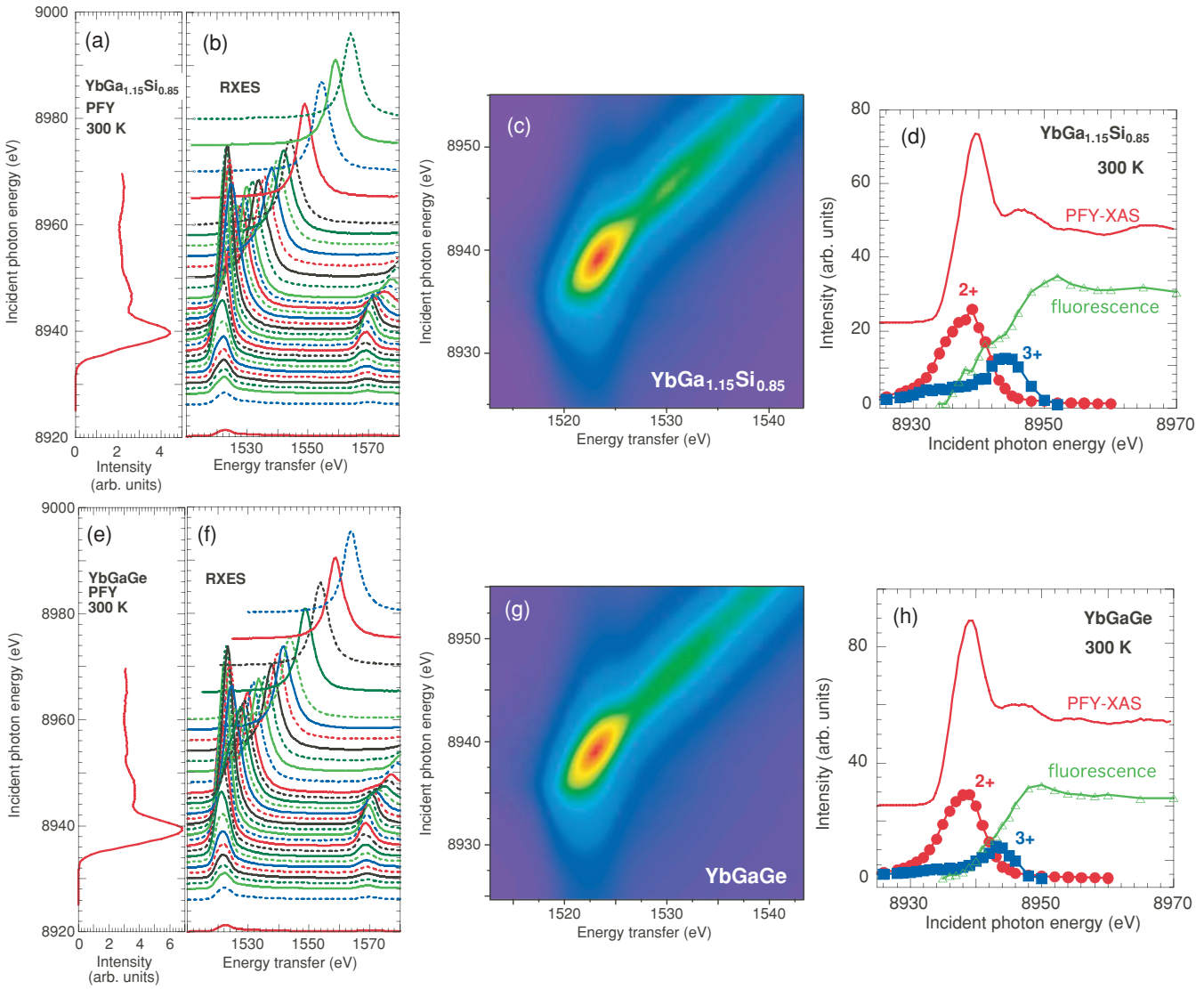

FIG. 2. (Color online) (a) and (e) PFY-XAS spectra for $YbGa_{1.15}Si_{0.85}$ and YbGaGe at 300 K. (b) and (f) RXES spectra as a function of the incident photon energies. The vertical position of the each RXES spectra corresponds to the E_{in} of PFY-XAS spectrum they were measured at in the panels (a) and (e), respectively. (c) and (g) Contour images of the RXES spectra. (d) and (h) Analyzed results of the Raman and fluorescence components as a function of the incident photon energies by the fitting procedure with the PFY-XAS spectra. Closed circles and closed squares correspond to the $2+$ and $3+$ components, respectively.

Figures 2(b) and 2(f), respectively, show the RXES spectra measured on $YbGa_{1.15}Si_{0.85}$ and YbGaGe at 300 K, as a function of the incident energy across the Yb L_3 edge. The vertical offset of the RXES spectra is scaled to the incident energy axis of the PFY-XAS spectrum [Figs. 2(a) and 2(e)]. Figures 2(c) and 2(g) reveal the contour images of the RXES spectra. Energy transfer is defined as the difference between the incident photon (E_{in}) and the emitted photon energies. Each RXES spectrum is fitted with three components corresponding to the Raman Yb^{2+} ($4f^{14}$) and Yb^{3+} ($4f^{13}$) and the fluorescence, assuming two Voigt functions.[22,27,28] In the Raman spectra below the absorption edge the Yb^{3+} contribution is small, but necessary to a proper fit. Figures 2(d) and 2(h) show the results of the analysis. We estimated the mean valence by using the formula $v = 2 + I(f^{13})/\{I(f^{13}) + I(f^{14})\}$, where $I(f^n)$ is the intensity of the f^n component. The valences are estimated to be $v = 2.38 \pm 0.03$ and 2.32 ± 0.03 for $YbGa_{1.15}Si_{0.85}$ and YbGaGe, respectively, which are consistent with previous estimations using PFY-XAS for $YbGa_xSi_{2-x}$ ($x = 1.2$, 1.3, 1.4) (Ref. 12). The valence is comparable for YbGaSi and YbGaGe, suggesting that there is no critical change of the electronic structure between these two systems. The values of the valence estimated from the fits to PFY-XAS spectra, as will be shown below, are lower than the RXES-derived values. This difference can usually be ascribed to the uncertainty of the PFY-XAS analysis due to the overlap of the $2p \rightarrow 5d$ peaks with the arctan-like part corresponding to the excitations toward the continuum. We note that although this uncertainty may affect the absolute value of the valence, the estimation of the relative changes as a function of temperature or pressure remains reliable.[27] We also note that an analysis of the magnetic susceptibility data of $YbGa_xSi_{2-x}$ using the Curie-Weiss law suggested that Yb is divalent.[12] We also note that in $YbGa_xSi_{2-x}$ the magnetic susceptibility measurement

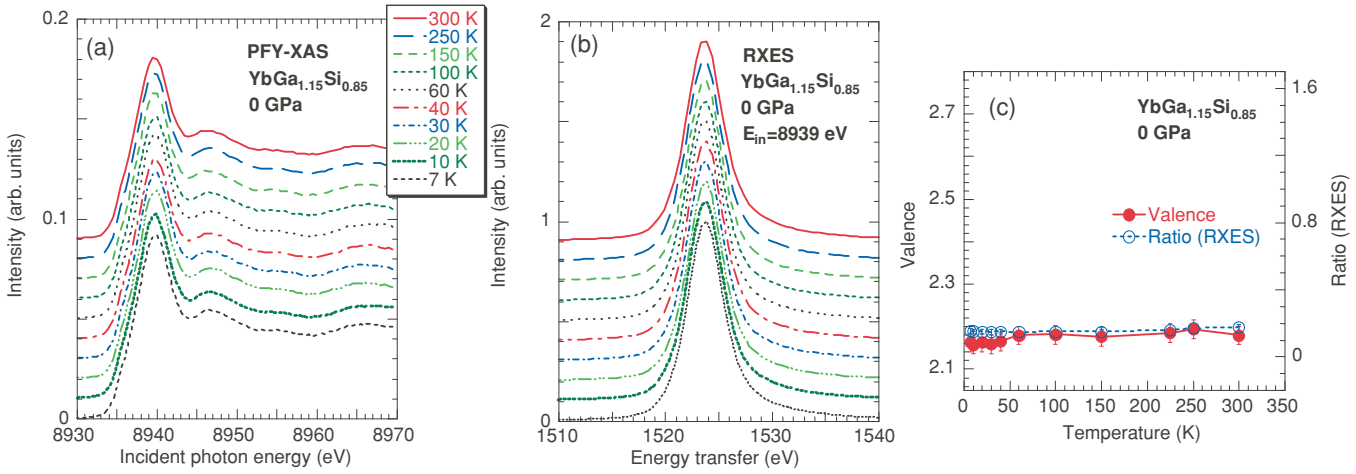

FIG. 3. (Color online) Temperature dependence of (a) the PFY-XAS spectra, (b) RXES spectra, and (c) valence for $YbGa_{1.15}Si_{0.85}$.

suggested a much smaller valence compared to the one obtained by RXES and the ground state mostly consists of Yb^{2+} (Ref. 12). Our PES measurement shows similar values of the valences as RXES as will be shown below. A possible explanation for this matter is that the Yb^{3+} states are only observable in the RXES or PES and originated by the *valence fluctuation* with short lives, leading to a lower susceptibility because the time scale in the measurement of the susceptibility is much longer than that of the valence fluctuation.[12,32] Another possible explanation is that when valence fluctuation occurs, Curie-Weiss behavior is only expected at temperatures above the characteristic temperature related to the strength of the c-f hybridization and the Curie-Weiss fitting does not yield the exact valence. As will be shown in the next section, no temperature dependence of the valence is observed between 7 and 300 K, suggesting that the characteristic temperature is higher than room temperature. This explains the discrepancy with the x-ray spectroscopic study.[12]

B. PFY-XAS and RXES: Temperature and pressure dependences

We now turn to the temperature and pressure dependences of the PFY-XAS and RXES spectra. Figures 3(a)–3(c) show the temperature dependence of the PFY-XAS spectra, of the RXES spectrum measured at $E_{in} = 8939$ eV, and of the valence for $YbGa_{1.15}Si_{0.85}$, respectively. The RXES spectra in Fig. 3(b) consist mainly of Yb^{2+} and a small fraction of Yb^{3+} on the high energy-transfer side as described above. No temperature dependence is observed for both PFY-XAS and RXES spectra, and accordingly for the valence, from room temperature down to 7 K within an accuracy of a few %. Doyle *et al.*[20] measured the valence-band spectra for YbGaGe as a function of the temperature from room temperature to 115 K. The PES spectra and the Yb valence did not show temperature dependence. Our results indicate that the impurity Anderson model picture[27] should be ruled out. We consider that in YbGaGe and YbGaSi the energy level of Yb^{2+} state may be lower than that of Yb^{3+} state and Yb^{2+} is preferred as a ground state. As a result, Yb in YbGaGe and YbGaSi behaves electronically as a divalent ion at room temperature, and lowering the temperature cannot result in decreasing the valence.

Figures 4(a)–4(c) present the pressure dependence of the PFY-XAS spectra, the RXES spectra, and the valence, respectively. The Yb^{3+} component in both PFY-XAS and RXES spectra increases drastically with pressure. The valence, estimated from the PFY-XAS spectra, increases steadily with pressure to around 10 GPa, beyond which it saturates to $v \sim 2.55$. Pressure therefore induces a gradual transition from the non-magnetic Yb^{2+} state to the magnetic Yb^{3+} state with

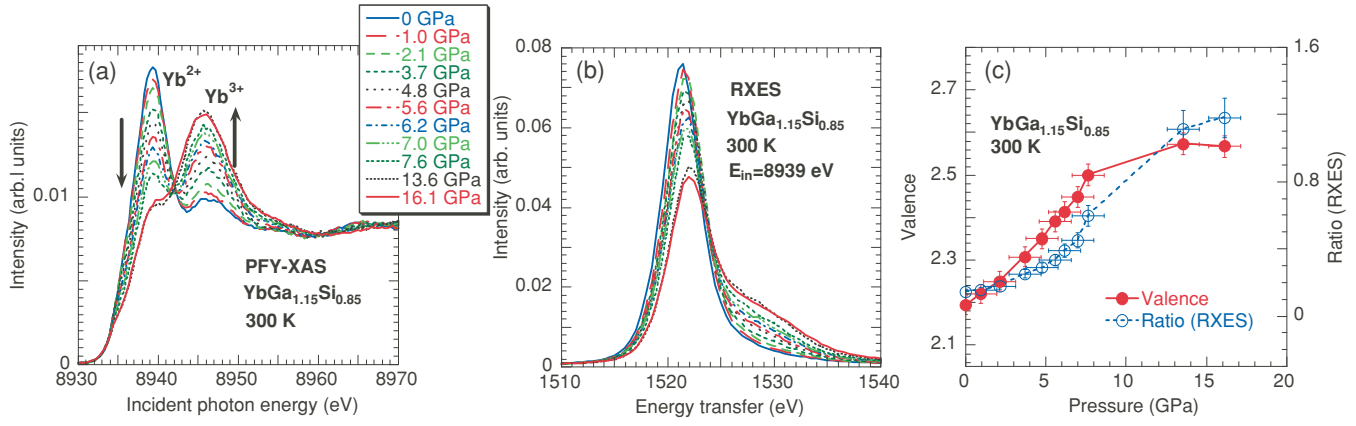

FIG. 4. (Color online) Pressure dependence of (a) the PFY-XAS spectra, (b) RXES spectra, and (c) valence for $YbGa_{1.15}Si_{0.85}$.

pressure in $YbGa_{1.15}Si_{0.85}$. No first-order valence transition is observed, hinting that no the valence increase is not linked to a structural transition. In Yb systems the magnetic Yb^{3+} component is normally favored at high pressure as observed in other Yb systems.[33–35] A dynamical mean-field (DMF) calculation showed gradual transition from $4f^{14}$ to $4f^{13}$ states.[36] Accordingly, one may expect the valence transition from a weakly hybridized and nearly nonmagnetic ground state (Yb^{2+}, $4f^{14}$) to a magnetic ground state (Yb^{3+}, $4f^{13}$) with pressure as observed in Yb metal.[37] But at present we do not understand why Yb valence saturates around $v \sim 2.55$. It is important to note that normally the superconducting state is destroyed as the magnetic component increases. In practice the decrease of T_C with pressure in $YbGa_{1.1}Si_{0.9}$ has been recently observed.[38] For YbGaGe we may expect a similar pressure dependence of the valence to $YbGa_{1.15}Si_{0.85}$ since the overall electronic structure is similar.

C. PES: valence band spectra

We used PES to obtain information about the electronic structure in a complementary way to RXES at ambient pressure. We measured the valence band spectra at both $E_{in} = 1100$ and 35 eV for the superconductor and non-superconductor. Valence-band photoelectron spectra obtained for $YbGa_{1.15}Si_{0.85}$ and $YbGa_{1.1}Ge_{0.9}$ at $E_{in} = 1100$ eV and 50 K are shown in Figs. 5(a) and 5(b). The resolution is $\Delta E \simeq 0.2$ eV. The intensity is normalized to the maximum of the strongest line. Note that although we measure the $YbGa_{1.1}Ge_{0.9}$ sample with similar chemical composition to $YbGa_{1.15}Si_{0.85}$ for comparison, it is reported that the Yb valence is insensitive to the chemical composition in $YbGa_xGe_{2-x}$ (Ref. 19). For both samples Yb mainly consists of Yb^{2+} component with a small fraction of Yb^{3+} component. Yb^{2+} component splits into the Yb $4f_{7/2}$ around $E_b = 0.3$ eV and the Yb $4f_{5/2}$ around the binding energy of $E_b = 1.5$ eV due to the spin-orbit interaction. Yb^{3+} is located from 6 to 12 eV and consists of the intraatomic multiplet structure. In the Yb system, surface effect is observed as an increase of the tail at the higher binding energy side. The valence is estimated from the integral intensity of each Yb component to be 2.27 ± 0.03 and 2.24 ± 0.03 for $YbGa_{1.15}Si_{0.85}$ and $YbGa_{1.1}Ge_{0.9}$, respectively, after subtracting the surface components. These values are comparable within experimental errors to 2.29 ± 0.015 estimated by Doyle *et al.*[20] for YbGaGe and the ones obtained from our RXES measurement.

The valence-band spectra around Yb^{3+} peaks is shown in Fig. 5(b) with an atomic model calculation for Yb^{3+}, adjusting the binding energy of the calculated spectrum to the experimental result. Note that the resolution of the spectra is about 0.4 eV for $YbGa_{1.1}Ge_{0.9}$ and 0.2 eV for $YbGa_{1.15}Si_{0.85}$. In the calculation of the Yb $4f$ spectra the Slater integrals and the spin-orbit coupling constants are calculated by Cowan's Hartree-Fock program with relativistic corrections[39] and Slater integrals scaled down to 90%. The atomic model calculation is found to satisfactorily reproduce the experimental result, indicating localized Yb^{3+} state. Doyle *et al.* reported a similar Yb^{3+} $4f$ spectra for YbGaGe (Fig. 5 in Ref. 20). In our spectra in Fig. 5 we observe a peak around $E_b = 16$ eV. In $YbBi_3$ this peak was identified to be a plasmon satellite.[40]

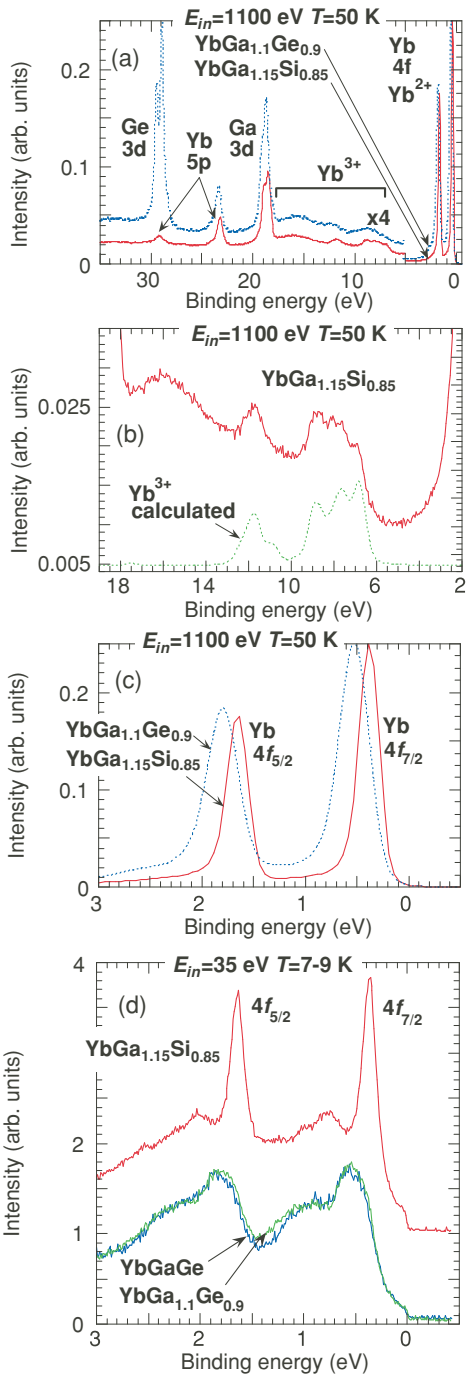

FIG. 5. (Color online) (a) The valence-band spectra of $YbGa_{1.15}Si_{0.85}$ and $YbGa_{1.1}Ge_{0.9}$ at the incident photon energy of $E_{in} = 1100$ eV and 50 K. (b) Expanded view of the valence-band spectra for (a) around Yb^{3+} peaks. Yb^{3+} spectra based on the atomic model calculation are also shown. (c) Valence-band spectra at $E_{in} = 1100$ eV and 50 K. (d) High-resolution valence-band spectra at $E_{in} = 35$ eV and 7–9 K.

Figures 5(c) and 5(d) show the valence-band spectra at $E_{in} = 1100$ eV with $\Delta E \simeq 200$ meV and at $E_{in} = 35$ eV with $\Delta E \simeq 10$ meV, respectively. Figure 5(d) shows that x dependence of the spectra is little. A slight difference between the valence-band spectra of $YbGa_{1.15}Si_{0.85}$ and $YbGa_xGe_{2-x}$ is discernible in the vicinity of the Fermi edge. In Fig. 5(d)

the broad peaks at higher binding energy correspond to the surface electronic states. In Fig. 5(d) one can clearly identify the density of states (DOS) at the Fermi edge (ϵ_F) in agreement with the metallic conductivity of these compounds. The Fermi edge is not clearly observed when taken at $E_{in} = 1100$ eV since the photoionization cross-sections for the s, p, d orbitals forming the conduction bands are much weaker than that for the Yb $4f$ orbital. At $E_{in} = 9$ eV these bulk $4f$ peaks (not shown here) are more suppressed and almost no bulk $4f$ peak is observed in $YbGa_xGe_{2-x}$. This could be explained because as the energy goes to 9 from 35 eV, the $4f$ photoionization cross-section decreases, while those of Ga $4p$, Ge $4p$, and Si $3p$ increase in a log-scale.[41]

The Kondo resonance peak at the Fermi edge appears as a result of the hybridization (i.e., in a mixed valence system the Yb^{2+} $4f_{7/2}$ peak is located at ϵ_F if the hybridization is strong[42]). However, in the valence band spectra of $YbGa_xSi_{2-x}$ and $YbGa_xGe_{2-x}$ the $4f_{7/2}$ peak is away from ϵ_F, hence it cannot be attributed to the Kondo resonance peak. A preliminary result of the electronic specific coefficient (γ) is 10 mJ/(mol K^2) for $YbGa_{1.1}Si_{0.9}$ (Ref. 38), which is slightly larger than the values of 3.56 mJ/(mol K^2) for CaGaSi (Ref. 43) and 6.1 mJ/(mol K^2) for CaAlSi (Ref. 44). These systems seem to not be heavy Fermion systems and this may explain the absence of the Kondo resonance peak in $YbGa_xSi_{2-x}$. It is noted that although in YbGaSi the hybridization is small, the above difference of the γ may be induced by the weak hybridization of Yb sites.

Now we discuss the DOS at ϵ_F, which affects the superconductivity in the BCS theory. In EuGaSi and EuGaGe (Ref. 13) the band calculation showed that the DOS at ϵ_F mainly consists of Eu $5d$ band as well as the case of M $5d$ band in $M(Ga_{0.5}Si_{0.5})_2$ (M = Ca, Sr, Ba) (Ref. 45). Therefore we suppose that the DOS at ϵ_F in Fig. 5(d) is attributed to the Yb $5d$ band with a small fraction of the GaSi or GaGe sp band. On the other hand, the tail of Yb $4f_{7/2}$ peak seems to increase the DOS at ϵ_F. In the BCS theory higher DOS at ϵ_F induces higher T_C. In EuGaSi no superconducting state is observed although it has the same crystal structure as YbGaSi. The overlap of the tail of $4f_{7/2}$ component at lower binding energy and relatively higher DOS at ϵ_F compared to YbGaGe may be one of the possible reasons in the advent of the superconductivity in YbGaSi. The sharp $4f$ DOS partly overlaps with the wide d band at ϵ_F. This seems also to be responsible of the fact that T_C shows a relatively large pressure derivative of $d \ln T_C/dP$, where P is the pressure, if the overlapped part decreases with pressure.[38] But the DMF calculation showed that Yb $4f^{7/2}$ peak shifted toward the Fermi level and the DOS at ϵ_F increased with pressure.[36] This is inconsistent with the above scenario. If we follow the DMF calculation, our result may suggest that the effect of the increase of the Yb^{3+} magnetic component and the deformation of the crystal structure with pressure may exceed that of the increase of the DOS at ϵ_F. We should note that in the bulk sensitive spectra at $E_{in} = 1100$ eV in Fig. 5(c) the Yb $4f^{2+}$ line width of $YbGa_{1.15}Ge_{0.85}$ is broader than that of $YbGa_{1.1}Si_{0.9}$. A similar relation is also observable in the spectra at $E_{in} = 35$ eV in Fig. 5(d), although the bulk sensitive spectra shows more pronounced intensity for $4f$ components. Figure 5(d) shows that the binding energies of the $4f$ peaks in $YbGa_xGe_{2-x}$ shifts to higher energies by about 0.18 eV. The DOS at ϵ_F in $YbGa_xGe_{2-x}$ appears to be smaller than those in $YbGa_{1.15}Ge_{0.85}$. These apparent differences of the electronic structures may be caused by the difference of the crystal structures. The in-plane lattice constant a of $YbGa_xGe_{2-x}$ is always larger than that of $YbGa_xSi_{2-x}$, while the mean interlayer distance of $YbGa_xGe_{2-x}$ is smaller than that of $YbGa_xSi_{2-x}$ (Refs. 12 and 19). Furthermore the shortest Ga-Ga distance as well as Yb-Ga distance in $YbGa_xGe_{2-x}$ is shorter than that in $YbGa_xSi_{2-x}$. Thus in $YbGa_xGe_{2-x}$, compared to $YbGa_xSi_{2-x}$, $4f$ bandwidth may be wider and the Fermi level raised. It is, therefore, considered that these differences in the crystal structure cause the difference observed in the valence-band spectra.

D. Resonant PES for $YbGa_{1.15}Si_{0.85}$

We present our resonant PES data obtained on the superconductor. The measurements of the resonant valence-band spectra as a function of the incident photon energies are performed at Yb $3d$ and Ga $2p$ absorption edges, as shown in Figs. 6(a) through 6(e) with the total electron yield spectra, corresponding to the x-ray absorption spectra. The spectra obtained by resonant PES are comparable to those obtained by RXES, with both Raman-like and fluorescence-like (or Auger-like) spectral features at the absorption edge.[46–49] The intensity in Figs. 6(b) and 6(e) is normalized by the incident photon beam intensity. In Fig. 6(c) the intensity is normalized to the maximum line intensity to see the Auger lines. At the Yb $3d$ absorption edge the resonant enhancement of the Yb^{2+} and Yb^{3+} line intensity is observed. In Yb^{3+} $3d$-$4f$ resonant absorption can occur and weak Yb^{3+} peaks are observable in Figs. 6(b), 6(c), and 6(e). Yb^{3+} has a multiplet structure of ^1S, ^1D, ^1G, ^1I, ^3P, ^3F, and ^3H. The peaks around 5 eV mainly consist of ^1G, ^3F, and ^3H and in the peaks around 12 eV ^3P and ^1I components are selectively enhanced.[50] In the inserted figure of Fig. 6(c) we observe fluorescence-like behavior of the normal Auger lines, shifting the binding energy in proportion to the incident energies. The Auger line intensity corresponds to the intensity of the XAS and is very weak compared to the intensity observed in the $3d$ compounds.[30] Around Yb $3d$ absorption edge Raman-like resonant Auger is not observed due to the overlap with the strong Yb^{2+} lines. In this region the process of the resonant photoelectrons is also superior to the contribution of the resonant Auger process. On the contrary to the resonant PES at Yb $3d$ edge we did not observe the resonant effect on the Ga $2p_{3/2}$ spectra as shown in Fig. 6(e). This may be explained if the width of the conduction band in the final states of the photoabsorption is broad, because the resonant effect is enhanced depending on the degree of the localization in the final states, indicating significant mixing between Ga and Si orbitals.

Figure 7 shows constant initial state (CIS) spectra at given binding energies as a function of the incident photon energies. At the binding energies corresponding to Yb^{2+} peaks the intensity of the CIS spectra roughly follows the change in the intensity of Yb $3d$ XAS, and a weak Fano-like profile is observed.[29,50,51] On the other hand, the intensity of the CIS for Yb^{3+} ($4f^{13}$) peaks is largely enhanced asshown in the inset of Fig. 7. The electron emissions from the Raman-like direct process and the photoabsorption process followed by a super

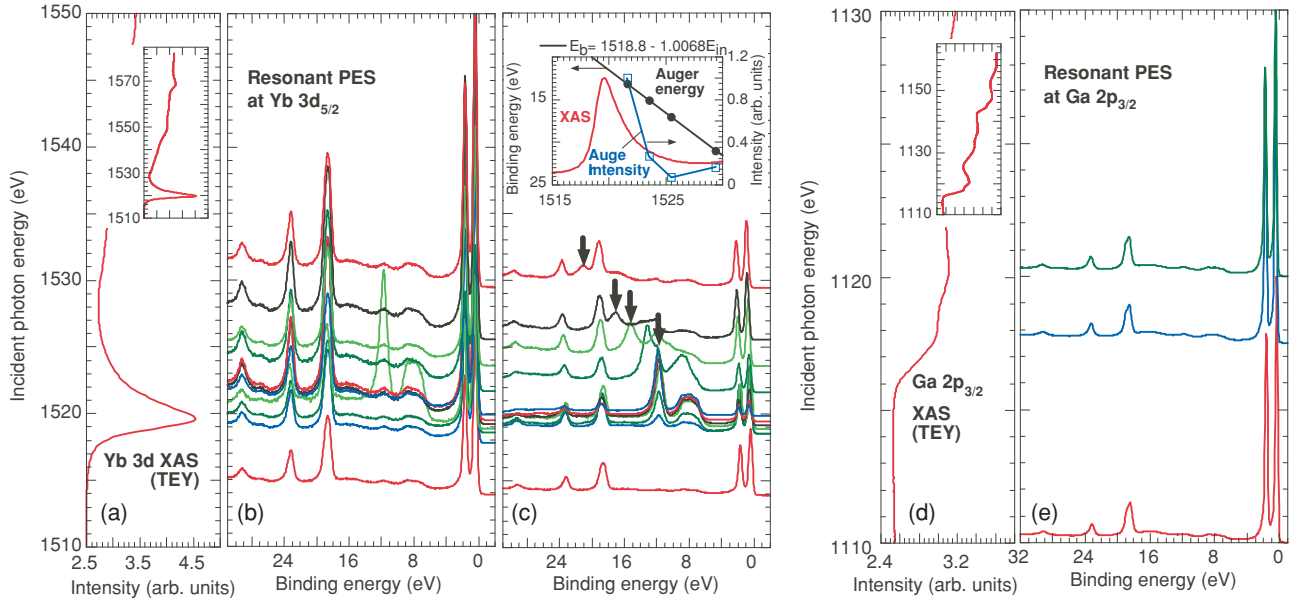

FIG. 6. (Color online) Resonant valence-band spectra for $YbGa_{1.15}Si_{0.85}$ at 50 K; (a)–(c) at Yb $3d$ absorption edge and (d) and (e) at Ga $2p_{3/2}$ absorption edge with total electron yield (TEY) spectra, corresponding x-ray absorption spectra (XAS). The vertical position of the resonant valence-band spectra in the left panel with regards to the absorption spectrum in the right panel corresponds to the incident energy they were collected at. The PFY-XAS spectra with wide incident energy range is also shown in the inset figures of (a) and (d). The intensity is normalized by the incident beam intensity in (b) and (e), and by the maximum intensity to see the Auger lines in (c). In (c) inset figure shows the incident energy (E_{in}) dependence of the binding energy and intensity of the Auger lines. Arrows in (c) are Auger lines.

Coster-Kronig Auger decay are, respectively, written as $h\nu + 3d^{10}4f^n \rightarrow 3d^{10}4f^{n-1} + e_k$ and $h\nu + 3d^{10}4f^n \rightarrow 3d^94f^{n+1} \rightarrow 3d^{10}4f^{n-1} + e_k$, where e_k is the emitted electrons. In photoelectron emission E_b is constant below the absorption edge, indicating Raman-like behavior, and this is one-step or coherent process. E_b of Auger process is proportional to the incident photon energies, corresponding fluorescence-like two-step or incoherent process. The interaction may occur between the discrete state ($3d^94f^{n+1}$) and the continuum state ($3d^{10}4f^{n-1} + e_k$). They have the same initial and final states and thus the Fano-like profile could be observable if two processes are mixed. The Fano-like profile in the CIS spectra indicates the discrete intermediate excited states and localized electronic structure. In the CIS spectra of Yb^{2+} the Fano-like profile is more clear compared to Yb^{3+} CIS. It is reasonable that the resonant $3d$-$4f$ transition occurs strongly for the Yb^{3+} component, which has an unfilled $4f$ site. On the other hand, the weak resonant behavior in Yb^{2+} indicates the hybridization between the Yb $4f$ and GaSi p band because Yb^{2+} ($4f^{14}$) has a closed shell structure and the resonant enhancement should occur only through the weakly hybridized p band. This scenario is consistent with the RXES measurement that states that a small part of Yb^{2+} states include the hybridized states.

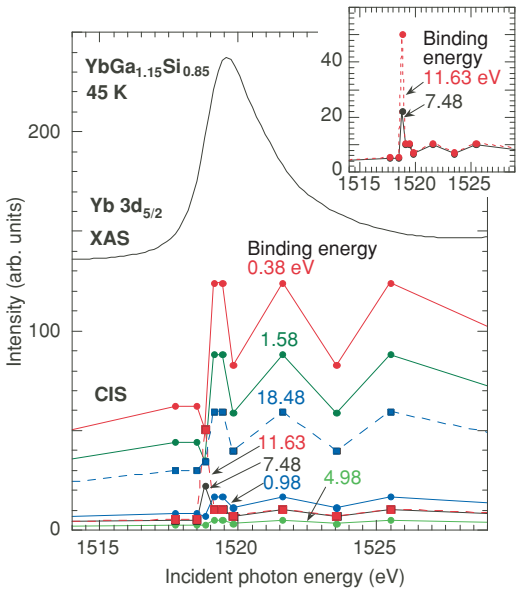

FIG. 7. (Color online) Constant initial state (CIS) spectra at given binding energies as a function of the incident photon energies for $YbGa_{1.15}Si_{0.85}$ at 50 K, obtained from the data in Fig. 6, with XAS spectrum at Yb $3d$ absorption edge. Right-upper panel shows the extended figure for the spectra at the binding energies of 7.48 and 11.63 eV, corresponding Yb^{3+} peaks [see Fig. 5(a)].

E. Relation between superconductivity and the electronic and crystal structures

We now discuss the relation between superconductivity and the crystal and electronic structures. First we discuss the possibility to have the modification of the electronic structure responsible for the suppression of the superconductivity. Both measurements of the RXES and resonant PES indicate that the superconductor $YbGa_xSi_{2-x}$ system is in the mixed valence state. The increase of the valence (i.e., increase of the magnetic Yb^{3+} component) may be related to the decrease of

the superconducting transition temperature in $YbGa_xSi_{2-x}$. Such suppression of T_C due to the c-f hybridization had been also reported in $YbNi_2B_2C$ (Refs. 52 and 53) and $Y_{1-x}Pr_xBa_2Cu_3O_7$ (Ref. 25). In $YbGa_xSi_{2-x}$ the carriers of the superconductor are electrons, the increase of Yb valence corresponds to a doping of the electrons to the conduction band, and thus over-doping of the electrons may destroy the superconductivity. Now we discuss the charge assignment in $YbGa_xSi_{2-x}$ using the Zintl-Klemm formula which can be written as $Yb^{v+}Ga_x^{1-}Si_{2-x}^{0+} \cdot (v-x)e^-$ (Refs. 12 and 54). This corresponds to a total electron number of $v+3x+4(2-x)$, eight valence electrons are in the Ga-Si layer and there are $(v\text{-}x)$ extra electrons, contributing to the conductivity. We note that for $YbGa_xGe_{2-x}$ the same relation is kept. On the other hand, the valence of YbGaSi is apparently larger than that of YbGaGe as shown in Fig. 1. Similar relation to the valence is deduced form the RXES and PES analysis on $YbGa_{1.15}Si_{0.85}$ and $YbGa_xGe_{2-x}$. A slight difference of the Yb valence between $YbGa_xSi_{2-x}$ and $YbGa_xGe_{2-x}$ is likely to originate from the difference in the crystal structure. Temperature dependence of the Yb valence for $YbGa_{1.15}Si_{0.85}$ is not observed as well as for YbGaGe. These facts indicate that the valence states of these compounds are very similar and the scenario of Cooper-pair breaking due to the local magnetic moment of Yb to explain the absence of superconductivity in YbGaGe is ruled out.

Next we consider the suppression of the superconductivity from the viewpoint of the crystal structure. YbGaSi has AlB_2-type crystal structure with the Ga-Si honeycomb layer, while YbGaGe shows the puckered Ga-Ge layer structure as shown in Fig. 1(b). The difference in the valence-band spectra between $YbGa_{1.15}Si_{0.85}$ and $YbGa_xGe_{2-x}$ in Fig. 5 may be attributed to the difference of these crystal structures. Our results show that the difference of the crystal structure may be crucial in the advent of the superconductivity in $YbGa_xSi_{2-x}$. We found that the pressure changes the Yb valence from divalent to trivalent states gradually. It is considered that the over-doping of the electrons to the superconducting Ga-Si layer in the pressure dependence may directly destroy the superconductivity. But the valence band spectra also suggest another possible scenario in which the sharp $4f$ DOS is partly overlapping with the wide d band at ϵ_F, the shift of the $4f$ level with pressure decrease the DOS at ϵ_F, and thus T_C decrease. On the other hand, as mentioned above in $YbGa_xSi_{2-x}$ T_C decreases with increasing x (Ref. 12). The lattice constants and the volume increased with x monotonically and the crystal structure did not change. The relation between the volume and T_C in x dependence seems to be in contrast with the pressure dependence. Here it is interesting to note that recently in iron pnictide superconductors the deviation from optimum crystal structure causes to decrease T_C (Refs. 55 and 56). Thus similar to the iron pnictide superconductors the increase of x may induce the deviation from the optimum crystal structure and the decrease of T_C.

IV. CONCLUSION

The electronic structure of superconductor $YbGa_{1.15}Si_{0.85}$ has been measured using two hard x-ray spectroscopic probes, having bulk sensitivity, PFY-XAS and RXES at the Yb L_3 edge. We also measure nonsuperconductor $YbGa_xGe_{2-x}$ for comparison. Complementary to the RXES, the soft x-ray and UV PES have been performed. Yb valence is nearly divalent, indicating nonmagnetic ground state with a small fraction of trivalent state at ambient pressure. No temperature dependence of the valence for $YbGa_{1.15}Si_{0.85}$ is observed in the PFY-XAS and RXES spectra at the temperature range of 7–300 K, as well as in YbGaGe. We found strong pressure dependence of the valence in $YbGa_{1.15}Si_{0.85}$ that the valence gradually increases with pressure similar to Yb metal and saturates to be $v \sim 2.55$ above 13 GPa. Valence band spectra for $YbGa_{1.15}Si_{0.85}$ show that the sharp $4f$ DOS is partly overlapping with the wide d band at ϵ_F, which may be responsible for the fact that pressure dependence of T_C showed relatively large $d \ln T_C/dP$. The resonant PES for $YbGa_{1.15}Si_{0.85}$ shows that in the CIS spectral intensity of Yb^{3+} is strongly enhanced at the Yb $3d$ absorption edge. Very weak resonant behavior in the CIS spectra for Yb^{2+} component of $YbGa_{1.15}Si_{0.85}$ indicates that Yb^{2+} state includes a small part of hybridized state. In the valence band spectra for $YbGa_{1.15}Si_{0.85}$ the Kondo resonant peak is not observable clearly, also indicating the weak hybridization. The measurements of the RXES and PES show that the valences are similar for both superconductor $YbGa_{1.15}Si_{0.85}$ and nonsuperconductor $YbGa_xGe_{2-x}$, although the crystal structure of the AlB_2 type in YbGaSi is different from that of the YPtAs type in YbGaGe. We found the difference between $YbGa_{1.15}Si_{0.85}$ and $YbGa_xGe_{2-x}$ in the valence-band spectra near the Fermi edge, which may be caused by the difference in the crystal structure. Our results indicate that the flat Ga-Si layered crystal structure with intercalated atoms may be important in the advent of the superconductivity in YbGaSi.

ACKNOWLEDGMENTS

The experiments were performed at RIKEN beamline BL17SU (RIKEN under Proposal No. 20080040) and Taiwan beamline BL12XU (SPring-8 under Proposal No. 2009A4255) at SPring-8, and at HiSOR beamline BL-9A (HiSOR under Proposal No. 10-A-47). This work is partly supported by Grant in Aid for Scientific Researches (Grant No. 22540343) from Ministry of Education, Culture, Sports, Science, and Technology of Japan. JFL acknowledges support from the Energy Frontier Research under Extreme Environments (EFree), the US National Science Foundation (EAR-0838221) and the Carnegie/DOE Alliance Center (CDAC).

[1] J. Nagamatsu, N. Nakagawa, T. Muranaka, Y. Zenitani, and J. Akimitsu, Nature (London) **410**, 63 (2001).

[2] T. E. Weller, M. Ellerby, S. S. Saxena, R. P. Smith, and N. T. Skipper, Nature Phys. **1**, 39 (2005).

[3] G. Csanyi, P. B. Littlewood, A. H. Nevidomsky, C. J. Pickard, and B. D. Simons, Nature Phys. **1**, 42 (2005).

[4] M. Imai, E. Abe, J. Ye, K. Nishida, T. Kimura, K. Honma, H. Abe, and H. Kitazawa, Phys. Rev. Lett. **87**, 077003 (2001).

[5] M. Imai, E. Abe, K. Nishida, T. Kimura, and H. Abe, Appl. Phys. Lett. **80**, 1019 (2002).

[6] M. Imai, K. Nishida, T. Kimura, and H. Abe, Physica C **377**, 96 (2002).

[7] M. Imai, K. Nishida, T. Kimura, H. Kitazawa, H. Abe, H. Kito, and K. Yoshii, Physica C **382**, 361 (2002).

[8] B. Lorenz, J. Lenzi, J. Cmaidalka, R. L. Meng, Y. Y. Sun, Y. Y. Xue, and C. W. Chu, Physica C **383**, 191 (2002).

[9] S. Yamanaka, T. Otsuki, T. Ide, H. Fukuoka, R. Kumashiro, T. Rachi, K. Tanigaki, F.-Z. Guo, and K. Kobayashi, Physica C **451**, 19 (2007).

[10] S. Kuroiwa, A. Q. R. Baron, T. Muranaka, R. Heid, K.-P. Bohnen, and J. Akimitsu, Phys. Rev. B **77**, 140503 (2008).

[11] M. Imai, A. Sato, T. Aoyagi, T. Kimura, Y. Matsushita, and N. Tsujii, J. Am. Chem. Soc. **130**, 2886 (2008), and references therein.

[12] N. Tsujii, M. Imai, H. Yamaoka, I. Jarrige, H. Oohashi, T. Tochio, K. Handa, J. Ide, H. Atsuta, Y. Ito, H. Yoshikawa, and H. Kitazawa, Chem. Mater. **22**, 4690 (2010).

[13] T.-S. You, Y. Grin, and G. J. Miller, Inorg. Chem. **46**, 8801 (2007).

[14] Y. Muro, T. Nakagawa, K. Umeo, M. Itoh, T. Suzuki, and T. Takabatake, J. Phys. Soc. Jpn. **75**, 1450 (2004).

[15] S. Bodev, D. J. Williams, J. D. Thompson, and J. L. Sarrao, Solid State Commun. **131**, 431 (2004).

[16] F. R. Drymiotis, Y. Lee, G. Lawes, J. C. Lashley, T. Kimura, S. M. Shapiro, A. Migliori, V. Correa, and R. A. Fisher, Phys. Rev. B **71**, 174304 (2005).

[17] K.-H. Jang, W. Y. Song, J.-G. Park, H. C. Kim, A. Lidbaum, H. Müller, and E. Bauer, Europhys. Lett. **69**, 88 (2005).

[18] Y. Janssen, S. Chang, B. K. Cho, A. Llobet, K. W. Dennis, R. W. McCallum, R. J. McQueeney, and P. C. Canfield, J. Alloys Compd. **389**, 10 (2005).

[19] N. Tsujii, T. Furubayashi, H. Kitazaswa, and G. Kido, J. Alloys Compd. **389**, 41 (2005).

[20] B. P. Doyle, E. Carleschi, E. Magnano, M. Malvestuto, A. A. Dee, A. S. Wills, Y. Janssen, and P. C. Canfield, Phys. Rev. B **75**, 235109 (2007).

[21] C. H. Booth, A. D. Christianson, J. M. Lawrence, L. D. Pham, J. C. Lashley, and F. R. Drymiotis, Phys. Rev. B **75**, 012301 (2007).

[22] I. Jarrige, H. Ishii, Y. Q. Cai, J.-P. Rueff, C. Bonnelle, T. Matsumura, and S. R. Shieh, Phys. Rev. B **72**, 075122 (2005).

[23] H. Yamaoka, M. Taguchi, A. M. Vlaicu, H. Oohashi, Y. Yokoi, D. Horiguchi, T. Tochio, Y. Ito, K. Kawatsura, K. Yamamoto, A. Chainani, S. Shin, M. Shiga, and H. Wada, J. Phys. Soc. Jpn. **75**, 034702 (2006).

[24] H. Yamaoka, N. Tsujii, K. Yamamoto, H. Oohashi, A. M. Vlaicu, K. Kunitani, K. Uotani, D. Horiguchi, T. Tochio, Y. Ito, and S. Shin, Phys. Rev. B **76**, 075130 (2007).

[25] H. Yamaoka, H. Oohashi, I. Jarrige, T. Terashima, Y. Zou, H. Mizota, S. Sakakura, T. Tochio, Y. Ito, E. Ya. Sherman, and A. Kotani, Phys. Rev. B **77**, 045135 (2008).

[26] H. Yamaoka, N. Tsujii, K. Yamamoto, A. M. Vlaicu, H. Oohashi, H. Yoshikawa, T. Tochio, Y. Ito, A. Chainani, and S. Shin, Phys. Rev. B **78**, 045127 (2008).

[27] H. Yamaoka, I. Jarrige, N. Tsujii, N. Hiraoka, H. Ishii, and K.-D. Tsuei, Phys. Rev. B **80**, 035120 (2009).

[28] H. Yamaoka, H. Sugiyama, Y. Kubozono, A. Kotani, R. Nouchi, A. M. Vlaicu, H. Oohashi, T. Tochio, Y. Ito, and H. Yoshikawa, Phys. Rev. B **80**, 205403 (2009).

[29] H. Yamaoka, M. Matsunami, R. Eguchi, Y. Ishida, N. Tsujii, Y. Takahashi, Y. Senba, H. Ohashi, and S. Shin, Phys. Rev. B **78**, 045125 (2008).

[30] H. Yamaoka, N. Tsujii, H. Oohashi, D. Nomoto, I. Jarrige, K. Takahiro, K. Ozaki, K. Kawatsura, and Y. Takahashi, Phys. Rev. B **77**, 115201 (2008).

[31] M. Arita, K. Shimada, H. Namatame, and M. Taniguchi, Surf. Rev. Lett. **9**, 535 (2002).

[32] B. C. Sales and D. K. Wohlleben, Phys. Rev. Lett. **35**, 1240 (1975).

[33] C. Dallera, E. Annese, J.-P. Rueff, A. Palenzona, G. Vankó, L. Braicovich, A. Shukla, and M. Grioni, Phys. Rev. B **68**, 245114 (2003).

[34] E. Annese, J.-P. Rueff, G. Vankó, M. Grioni, L. Braicovich, L. Degiorgi, R. Gusmeroli, and C. Dallera, Phys. Rev. B **70**, 075117 (2004).

[35] C. Dallera, O. Wessely, M. Colarieti-Tosti, O. Eriksson, R. Ahuja, B. Johansson, M. I. Katsnelson, E. Annese, J.-P. Rueff, G. Vankó, L. Braicovich, and M. Grioni, Phys. Rev. B **74**, 081101 (2006).

[36] E. R. Ylvisaker, J. Kunes, A. K. McMahan, and W. E. Pickett, Phys. Rev. Lett. **102**, 246401 (2009).

[37] A. Fuse, G. Nakamoto, M. Kurisu, N. Ishimatsu, and H. Tanida, J. Alloys Compd. **376**, 34 (2004).

[38] A. Ohmura, K. Fujimaki, M. Einaga, F. Ishikawa, A. Nakayama, Yuh Yamada, M. Imai, and N. Tsujii, J. Phys.: Conf. Ser. **215**, 012035 (2010).

[39] R. D. Cowan, *The Theory of Atomic Structure and Spectra* (University of California Press, Berkeley, CA, 1981).

[40] S. Suga, S. Ogawa, H. Namatame, M. Taniguchi, A. Kakizaki, T. Ishii, A. Fujimori, S-J. Oh, H. Kato, T. Miyahara, A. Ochiai, T. Suzuki, and T. Kasuya, J. Phys. Soc. Jpn. **58**, 4534 (1989).

[41] J. J. Yeh and I. Lindau, At. Data Nucl. Data Tables **32**, 1 (1985).

[42] M. Matsunami, A. Chainani, M. Taguchi, R. Eguchi, Y. Ishida, Y. Takata, H. Okamura, T. Nanba, M. Yabashi, K. Tamasaku, Y. Nishino, T. Ishikawa, Y. Senba, H. Ohashi, N. Tsujii, A. Ochiai, and S. Shin, Phys. Rev. B **78**, 195118 (2008).

[43] T. Tamegai, K. Uzato, S. Kashihara, T. Nakagawa, and M. Tokunaga, Physica C **426-431**, 208 (2005).

[44] S. Kuroiwa, H. Sagayama, T. Kakiuchi, H. Sawa, Y. Noda, and J. Akimitsu, Phys. Rev. B **74**, 014517 (2006).

[45] I. R. Shein, N. I. Medvedeva, and A. L. Ivanovskii, J. Phys. Condens. Matter **15**, L541 (2003).

[46] M. Weinelt, A. Nilsson, M. Magnuson, T. Wiell, N. Wassdahl, O. Karis, A. Föhlisch, N. Mårtensson, J. Stohr, and M. Samant, Phys. Rev. Lett. **78**, 967 (1997).

[47] M. Finazzi, G. Ghiringhelli, O. Tjernberg, Ph. Ohresser, and N. B. Brookes, Phys. Rev. B **61**, 4629 (2000).

[48] S. Hüfner, S.-H. Yang, B. S. Mun, C. S. Fadley, J. Schäfer, E. Rotenberg, and S. D. Kevan, Phys. Rev. B **61**, 12582 (2000).

[49] V. Formoso, G. Chiarello, R. G. Agostino, L. Papagno, E. Covavita, L. Floreano, R. Gotter, A. Morgante, A. Santaniello, and A. Verdini, Eur. Phys. J. B **43**, 463 (2005).

[50] L. I. Johansson, J. W. Allen, I. Lindau, M. H. Hecht, and S. B. M. Hagström, Phys. Rev. B **21**, 1408 (1980).

[51] M. Domke, C. Laubschat, E. V. Sampathkumaran, M. Prietsch, T. Mandel, G. Kaindl, and H. U. Middelmann, Phys. Rev. B **32**, 8002 (1985).

[52]S. K. Dhar, R. Nagarajan, Z. Hossain, E. Tominez, C. Godart, L. C. Gupta, and R. Vijayaraghavan, Solid State Commun. **98**, 985 (1996).

[53]A. Yatskar, N. K. Budraa, W. P. Beyermann, P. C. Canfield, and S. L. Budko, Phys. Rev. B **54**, R3772 (1996).

[54]T.-S. You, S. Ledin, O. Gourdon, Y. Wu, and G. J. Miller, Inorg. Chem. **48**, 6380 (2009).

[55]C. H. Lee, A. Iyo, H. Eisaki, H. Kito, M. T. Fernandez-Diaz, T. Ito, K. Kihou, H. Matsuhata, M. Braden, and K. Yamada, J. Phys. Soc. Jpn. **77**, 083704 (2008).

[56]H. Yamaoka, I. Jarrige, A. Ikeda Ohno, S. Tsutsui, J.-F. Lin, N. Takeshita, K. Miyazawa, A. Iyo, H. Kito, H. Eisaki, N. Hiraoka, H. Ishii, and K.-D. Tsuei, Phy. Rev. B **82**, 125123 (2010).